Overbounding Sequential Estimation Errors Due to Non-Gaussian Correlated Noise

Steven Langel*, *The MITRE Corporation*
Omar García Crespillo, *German Aerospace Center* (*DLR*)
Mathieu Joerger, *Virginia Tech*

BIOGRAPHIES

Steven Langel received a Ph.D. in mechanical and aerospace engineering from the Illinois Institute of Technology (IIT), Chicago, IL, USA. He is currently a lead signal processing engineer at The MITRE Corporation, Bedford, MA, USA, focusing on the development of multi-sensor navigation and fault detection algorithms. He is also pursuing research in robust estimation algorithms for safety-critical applications. Steve has been a member of the MITRE technical staff since 2014.

Omar García Crespillo holds an M.Sc. in Telecommunication Engineering from the University of Malaga in Spain. In 2013, he joined the Navigation department of the German Aerospace Center (DLR) where his current field of research includes multi-sensor fusion algorithms, GNSS, inertial sensors and integrity monitoring for safe ground and air transportation systems. Since 2015, he is also a PhD student at the Swiss Federal Institute of Technology (EPFL) in Lausanne.

Mathieu Joerger (M'14–SM'18) received the `Dipl\^ome d'Ingenieur' (Master degree) in Mechatronics from the National Institute of Applied Sciences, Strasbourg, France, the M.S. and Ph.D. degree in mechanical and aerospace engineering from the Illinois Institute of Technology (IIT), Chicago, IL, USA. He is currently an Assistant Professor of Aerospace and Ocean Engineering with Virginia Tech, Blacksburg, VA, USA, working on multisensor integration, on sequential fault-detection for multiconstellation navigation systems, and on receiver autonomous integrity monitoring for automotive and aviation applications. Prior to joining VT, he was an Assistant Professor at the University of Arizona, Tucson, AZ, and a Reseacrh Assistant Professor at IIT. Dr. Joerger is currently the Technical Editor of Navigation for IEEE Transactions on Aerospace \& Electronic Systems. He was the recipient of the Institute of Navigation (ION) Bradford Parkinson Award in 2009, and ION Early Achievement Award in 2014.

ABSTRACT

In this paper, we develop, analyze, and implement a new recursive method to conservatively account for non-Gaussian measurement errors with an uncertain correlation structure in Kalman filters (KFs). Under the assumptions of symmetric overbounding, the method guarantees a CDF overbound on the entire KF estimation error distribution. First, we leverage previous work on symmetric overbounding and frequency-domain overbounding to show how to transform a measurement domain CDF overbound into a position domain overbound. The second part of the paper evaluates the proposed method through Monte Carlo simulation for a GPS-based position estimation problem. Specifically, we show that while frequency domain overbounding produces a position domain overbound for Gaussian noise with an uncertain correlation structure, combination with symmetric overbounding is required to ensure position domain overbounding for non-Gaussian correlated noise.

INTRODUCTION

Safety-critical navigation applications must ensure that the probability of the estimation error exceeding predefined limits is acceptably small. This probability, often referred to as integrity risk, can be predicted to decide whether to proceed or continue with an operation.

---

* The author's affiliation with The MITRE Corporation is provided for identification purposes only and is not intended to convey or imply MITRE's concurrence with, or support for, the positions, opinions, or viewpoints expressed by the author.

For example, in order to determine whether to pursue or abort an aircraft landing using sensor information when the pilot has low visibility to the ground, it is crucial to upper bound the actual integrity risk. Failing to do so would provide optimistic, misleading, and hence unsafe information to users. In aviation applications, CDF overbounding has been used extensively to derive upper bounds on integrity risk for snapshot least-squares, GPS-based navigation.

Recursive filters can enable integration with additional sensors like an inertial measurement unit (IMU), which are instrumental in air, sea, and ground applications. They can also provide higher integrity performance than snapshot algorithms as illustrated for Advanced Receiver Autonomous Integrity Monitoring in [3]. Producing a guaranteed upper bound on integrity risk for sequential estimators is difficult because of uncertainty in characterizing time-correlated measurement errors like multipath. Precise multipath models are very difficult to obtain, as illustrated in [4] for an ensemble of empirically derived multipath autocorrelation sequences (ACSs). Thus, even using the best models available, there is an element of uncertainty when dealing with time-correlated noise.

CDF overbounding is attractive because it can account for non-Gaussian measurement errors. However, existing methods do not account for model uncertainty over time, which has prompted the development of new techniques. The symmetric overbounding (S.O) theorem was developed in [2] to extend CDF overbounding to linear systems where the measurement noise is correlated and could be non-Gaussian. The theorem assumes that each noise component can be expressed as the output of a linear system driven by spherically symmetric noise, and states that a CDF overbound on any noise component can be transformed into a CDF overbound on the estimation error distribution.

An upper bound on the estimation error variance is required for the transformation and can be difficult to obtain when time correlation models are uncertain. Reference [5] shows how to obtain the variance bound for a KF when the measurement noise ACSs are unknown but can be upper and lower bounded. The method requires storing matrices that grow after each KF update and can be a challenge to implement in real-time when high rate sensors like an IMU are being used. Without a practical method to obtain the variance bound, S.O has remained largely a topic of academic interest. In [1], we derived a new frequency-domain overbounding (F.D.O) method for specifying noise models that, when used in a state augmented KF, are guaranteed to produce a predicted estimation error variance that upper bounds the true variance. Like [5], F.D.O does not require knowledge of the underlying ACSs, but it has the additional advantage of enabling a variance bound to be defined recursively, opening the possibility for S.O to be incorporated in a real-time algorithm.

The first part of the paper merges S.O with F.D.O to create a practical method for overbounding KF-based estimation error distributions in the presence of time-correlated noise that may not be Gaussian. In the second part of the paper, we demonstrate the method using Monte Carlo simulation for a simplified GPS-based position estimation problem. We show that while F.D.O produces a position domain overbound for Gaussian noise with an uncertain correlation structure, combination with S.O is required to ensure position domain overbounding for non-Gaussian correlated noise.

PROBLEM STATEMENT

Consider the linear system

$$\begin{aligned} \boldsymbol{\xi}_{k+1} &= \mathbf{A}_k \boldsymbol{\xi}_k + \mathbf{B}_k \boldsymbol{w}_k \\ \boldsymbol{z}_k &= \mathbf{C}_k \boldsymbol{\xi}_k + \mathbf{D}_k \boldsymbol{v}_k \end{aligned} \tag{1}$$

where $\boldsymbol{\xi}_k$ is the state vector, $\boldsymbol{z}_k$ is the measurement vector, $\boldsymbol{w}_k \in \mathbb{R}^p$ and $\boldsymbol{v}_k \in \mathbb{R}^s$ are the process and measurement noise vectors, respectively, and $\mathbf{A}_k$, $\mathbf{B}_k$, $\mathbf{C}_k$ and $\mathbf{D}_k$ are known matrices of appropriate dimension. The components of $\boldsymbol{w}_k$ and $\boldsymbol{v}_k$ are mutually independent, have zero mean and are time-correlated with wide-sense stationary (WSS) ACSs. However, the exact structure of the measurement and process noise ACSs is unknown. It is also worth noting that the distribution of each component of $\boldsymbol{w}_k$ and $\boldsymbol{v}_k$ could be non-Gaussian, but we assume that the distributions are symmetric and unimodal.

Using $\boldsymbol{\eta}_K$ to denote a time series for an arbitrary process or measurement noise component from time index 0 to time index k, we assume that $\boldsymbol{\eta}_K$ can be expressed as $\boldsymbol{\eta}_K = \mathbf{G}_\eta \boldsymbol{\zeta}_K$, where $\boldsymbol{\zeta}_k$ is a spherically symmetric random process. That is, the probability density function (PDF) of $\boldsymbol{\zeta}_K$ is only dependent on $(\zeta_1^2 + \cdots + \zeta_k^2)$. The matrix $\mathbf{G}_\eta$ does not have to be known. Rather, it is enough to know that $\mathbf{G}_\eta$ exists. The significance of this assumption will be clear when we discuss overbounding in the presence of correlated noise. Given the assumptions above, we seek to develop a method for overbounding the KF-based estimate error distribution of $\boldsymbol{\xi}_k$.

ESTIMATE ERROR WITH MODEL UNCERTAINTY

Before tackling the overbounding problem, we need to define the KF estimate error vector $\boldsymbol{\varepsilon}_k$. Expressions for $\boldsymbol{\varepsilon}_k$ are well established for the ideal case where precise models are available for process and measurement noise. However, we rarely have access to such models, especially when the noise processes are time-correlated. Therefore, alternative expressions are needed to describe the propagation of $\boldsymbol{\varepsilon}_k$ when approximate noise models are used. Reference [6] derives these propagation equations for a KF that uses state augmentation to account for correlated noise, and this section summarizes those results.

State augmentation involves defining $\boldsymbol{w}_k$ and $\boldsymbol{v}_k$ as [7]

$$\begin{aligned} \boldsymbol{w}_k &= \mathbf{E}_{w,k}\boldsymbol{a}_k + \boldsymbol{n}_k \\ \boldsymbol{v}_k &= \mathbf{E}_{v,k}\boldsymbol{a}_k + \boldsymbol{r}_k \end{aligned} \quad , \quad \boldsymbol{a}_{k+1} = \mathbf{L}_k\boldsymbol{a}_k + \boldsymbol{u}_k \tag{2}$$

such that $\boldsymbol{n}_k$, $\boldsymbol{r}_k$ and $\boldsymbol{u}_k$ are zero-mean white noise processes with covariance matrices $\mathbf{N}_k$, $\mathbf{R}_k$ and $\mathbf{U}_k$. Substituting the expressions from Eq. (2) into Eq. (1) and appending $\boldsymbol{a}_k$ to $\boldsymbol{\xi}_k$ results in the new linear system

$$\begin{aligned} \begin{bmatrix} \boldsymbol{\xi}_{k+1} \\ \boldsymbol{a}_{k+1} \end{bmatrix} &= \begin{bmatrix} \mathbf{A}_k & \mathbf{B}_k\mathbf{E}_{w,k} \\ \mathbf{0} & \mathbf{L}_k \end{bmatrix} \begin{bmatrix} \boldsymbol{\xi}_k \\ \boldsymbol{a}_k \end{bmatrix} + \begin{bmatrix} \mathbf{B}_k\boldsymbol{n}_k \\ \boldsymbol{u}_k \end{bmatrix} \\ \boldsymbol{z}_k &= \begin{bmatrix} \mathbf{C}_k & \mathbf{D}_k\mathbf{E}_{v,k} \end{bmatrix} \begin{bmatrix} \boldsymbol{\xi}_k \\ \boldsymbol{a}_k \end{bmatrix} + \mathbf{D}_k\boldsymbol{r}_k \end{aligned} \tag{3}$$

which can be written more compactly as

$$\begin{aligned} \boldsymbol{x}_{k+1} &= \mathbf{F}_k\boldsymbol{x}_k + \boldsymbol{q}_k \\ \boldsymbol{z}_k &= \mathbf{H}_k\boldsymbol{x}_k + \mathbf{D}_k\boldsymbol{r}_k \end{aligned} \tag{4}$$

Since $\boldsymbol{q}_k$ and $\mathbf{D}_k\boldsymbol{r}_k$ are white random vectors, it is permissible to estimate $\boldsymbol{x}_k$ using a KF. When the actual noise distributions differ from the models in Eq. (2), the estimate error covariance matrix $\boldsymbol{\Sigma}_k$ provided by the KF is not the true covariance matrix. In fact, it is not possible to determine the entire estimate error vector under these circumstances. Instead, the best we can do is obtain propagation equations for the mixed vector $\boldsymbol{e}_k^T = \begin{bmatrix} \boldsymbol{\varepsilon}_{\xi,k}^T & \widehat{\boldsymbol{a}}_k^T \end{bmatrix}$, where $\boldsymbol{\varepsilon}_{\xi,k}$ is the estimate error vector for the states in $\boldsymbol{\xi}_k$ and $\widehat{\boldsymbol{a}}_k$ is the KF estimate of $\boldsymbol{a}_k$. This is not restrictive because we are only interested in overbounding components (or linear combinations of components) of $\boldsymbol{\xi}_k$. The sole purpose of including the states $\boldsymbol{a}_k$ is to transform Eq. (1) into a linear system driven by white noise so that it is permissible to use a KF for state estimation. Otherwise, they are nuisance states.

Reference [6] shows that $\boldsymbol{e}_k$ propagates according to

$$\begin{aligned} \boldsymbol{e}_{k+1|k} &= \mathbf{F}_k\boldsymbol{e}_{k|k} - \begin{bmatrix} \mathbf{B}_k \\ \mathbf{0} \end{bmatrix} \boldsymbol{w}_k \\ \boldsymbol{e}_{k|k} &= (\mathbf{I} - \mathbf{K}_k\mathbf{H}_k)\boldsymbol{e}_{k|k-1} + \mathbf{K}_k\mathbf{D}_k\boldsymbol{v}_k \end{aligned} \tag{5}$$

where $\mathbf{K}_k$ is the Kalman gain matrix and $\boldsymbol{e}_{k|k}$ is $\boldsymbol{e}$ at time index k based on all measurements up to and including time index k. The initial vector $\boldsymbol{e}_{0|0}$ is a zero-mean random vector with covariance matrix $\mathbf{P}_{0|0} = \begin{bmatrix} \mathbf{P}_{\xi,0} & \mathbf{0} \\ \mathbf{0} & \mathbf{0} \end{bmatrix}$ [6], where $\mathbf{P}_{\xi,0} = E[\boldsymbol{\varepsilon}_{\xi,0}\boldsymbol{\varepsilon}_{\xi,0}^T]$. We assume that $\boldsymbol{e}_{0|0}$ has a symmetric and unimodal PDF and that there exists a matrix $\mathbf{G}_e$ such that $\boldsymbol{e}_{0|0} = \mathbf{G}_e\boldsymbol{\zeta}_e$, where $\boldsymbol{\zeta}_e$ is a spherically symmetric random vector.

In what follows, we will focus on $\boldsymbol{e}_{k|k}$, but the results can just as easily be applied to $\boldsymbol{e}_{k|k-1}$. Equation (5) is not the most useful form because it hides the cross-correlation between $\boldsymbol{e}_{k|k}$, $\boldsymbol{w}_k$ and $\boldsymbol{v}_k$. Through successive substitution, another way to write $\boldsymbol{e}_{k|k}$ is [6]

$$\boldsymbol{e}_{k|k} = \boldsymbol{\Phi}_k\boldsymbol{e}_{0|0} + \sum_{i=1}^{p} \boldsymbol{\Gamma}_{ik}\boldsymbol{w}_{i,K-1} + \sum_{j=1}^{s} \boldsymbol{\Psi}_{jk}\boldsymbol{v}_{j,K} \tag{6}$$

where $\boldsymbol{w}_{i,K-1}$ is a time series of the i^{th} process noise component from time index 1 to time index $k-1$ and $\boldsymbol{\nu}_{j,K}$ is a time series of the j^{th} measurement noise component from time index 1 to time index k. We assume that $\boldsymbol{e}_{0|0}$ is independent of $\boldsymbol{w}_{i,K-1}$ and $\boldsymbol{\nu}_{j,K}$. This assumption if often valid in practice, but not always. Some components of the initial estimate vector $\hat{\boldsymbol{\xi}}_{0|0}$ could be obtained from an initial set of measurements $\boldsymbol{z}_0$, which would introduce correlation between $\boldsymbol{e}_{0|0}$ and $\boldsymbol{\nu}_0$ (and thus correlation between $\boldsymbol{e}_{0|0}$ and $\boldsymbol{\nu}_{j,K}$). One example where this occurs is in a GPS-based KF where the position estimate is initialized using snapshot least squares estimation with code phase measurements and an initial estimate of cycle ambiguities is obtained from a snapshot of carrier-minus-code measurements. In this case, we know the linear relationship between $\boldsymbol{e}_{0|0}$ and $\boldsymbol{\nu}_0$, which can be incorporated directly in Eq. (6). Thus, the independence assumption is not restrictive, and we will use it going forward to simplify the development.

Equation (6) conveniently expresses $\boldsymbol{e}_{k|k}$ as a sum of independent random vectors, but it is practically inconvenient because $\boldsymbol{\Gamma}_{ik}$ and $\boldsymbol{\Psi}_{jk}$ get bigger and bigger as time progresses. The reader should take comfort knowing that Eq. (6) will only be used as a vehicle to *develop* an overbounding strategy and will not play a role in the proposed overbounding method.

SYMMETRIC OVERBOUNDING

This section develops a methodology for obtaining a CDF overbound on any linear combination y_k of $\boldsymbol{e}_{k|k}$. From Eq. (6), y_k can generally be expressed as

$$y_k = \sum_{i=0}^{p+s} \boldsymbol{\alpha}_{ik}^T \boldsymbol{\eta}_{ik} \quad \text{with} \quad \boldsymbol{\eta}_{ik} = \begin{cases} \boldsymbol{e}_{0|0} & , \quad i = 0 \\ \boldsymbol{w}_{i,K-1} & , \quad i = 1, \dots, p \\ \boldsymbol{\nu}_{i-p,K} & , \quad i = p+1, \dots, p+s \end{cases} \tag{7}$$

Given that the $\boldsymbol{\eta}_{ik}$ are mutually independent with zero-mean, symmetric and unimodal distributions, [8] shows that if a CDF overbound can be defined for each of the $\boldsymbol{\alpha}_{ik}^T \boldsymbol{\eta}_{ik}$, then the convolution of these overbounds produces a CDF overbound on y_k, as long as the overbounds on $\boldsymbol{\alpha}_{ik}^T \boldsymbol{\eta}_{ik}$ are also zero-mean, symmetric and unimodal. Gaussian overbounds are mostly used due to their attractive properties (e.g., preservation through linear transformation and convolution). Thus, requiring overbounds that are zero-mean, symmetric, and unimodal is not too restrictive in practice. The difficulty is obtaining an overbound on $\boldsymbol{\alpha}_{ik}^T \boldsymbol{\eta}_{ik}$ when the components of $\boldsymbol{\eta}_{ik}$ are correlated.

For an arbitrary inner product $\varphi = \boldsymbol{\alpha}^T \boldsymbol{\eta}$, Eq. (20) in [2] shows that under the assumption that $\boldsymbol{\eta}$ can be expressed as $\boldsymbol{\eta} = \mathbf{G}\boldsymbol{\zeta}$, a CDF overbound $\bar{p}_{\eta_l}(\eta_l)$ on the l^{th} component of $\boldsymbol{\eta}$ can be transformed into an overbound on φ through

$$\bar{p}_{\varphi}(\varphi) = \frac{||\mathbf{G}_l||}{||\boldsymbol{\alpha}^T \mathbf{G}||} \bar{p}_{\eta_l}\left(\frac{||\mathbf{G}_l||}{||\boldsymbol{\alpha}^T \mathbf{G}||} \varphi \right) \tag{8}$$

such that $\mathbf{G}_l$ is the l^{th} row of $\mathbf{G}$ and $||\cdot||$ is the standard Euclidean norm. We refer to $\bar{p}_{\varphi}(\varphi)$ as a symmetric overbound (S.O) because it relies on the assumption that $\boldsymbol{\eta}$ can be mapped from a spherically symmetric space. The reader should be aware that Eq. (8) is the PDF corresponding to the S.O. This is standard practice for specifying CDF overbounds.

Equation (8) can be written a better way as follows. Without loss of generality, assume that the covariance matrix of $\boldsymbol{\zeta}$ is the identity matrix. Then from the relationship $\boldsymbol{\eta} = \mathbf{G}\boldsymbol{\zeta}$, the variance of the l^{th} component of η is $\sigma_{\eta_l}^2 = \mathbf{G}_l E[\boldsymbol{\zeta}\boldsymbol{\zeta}^T]\mathbf{G}_l^T = ||\mathbf{G}_l||^2$. Similarly, the variance of φ is given by $\sigma_{\varphi}^2 = \boldsymbol{\alpha}^T \mathbf{G} E[\boldsymbol{\zeta}\boldsymbol{\zeta}^T]\mathbf{G}^T\boldsymbol{\alpha}^T = ||\boldsymbol{\alpha}^T\mathbf{G}||^2$. Substituting these relations into Eq. (8) results in

$$\bar{p}_{\varphi}(\varphi) = \frac{\sigma_{\eta_l}}{\sigma_{\varphi}} \bar{p}_{\eta_l}\left(\frac{\sigma_{\eta_l}}{\sigma_{\varphi}} \varphi \right) \tag{9}$$

When σ_{η_l} and σ_{φ} are unknown (which will generally be the case), replacing them with a lower bound $\underline{\sigma}_{\eta_l}$ and an upper bound $\bar{\sigma}_{\varphi}$ will produce a distribution with heavier tails than $\bar{p}_{\varphi}(\varphi)$ and thus conservative assessments of integrity risk. To see this, write the PDF in Eq. (9) as $\bar{p}_{\varphi}(\varphi) = a\bar{p}_{\eta_l}(a\varphi)$ where $a \geq 0$. Integration leads to the CDF $\bar{F}_{\varphi}(\varphi) = \bar{F}_{\eta_l}(a\varphi)$. The left-hand tail probability $P(\varphi \leq \delta)$ is given by $\bar{F}_{\varphi}(\delta) = \bar{F}_{\eta_l}(a\delta)$. If a is replaced with a smaller value $\underline{a}$, the argument $\underline{a}\delta$ becomes greater

than $a\delta$, resulting in a larger value for $\bar{F}_{\eta_l}(a\delta)$. Thus, left-hand tail probabilities become larger when we use $\underline{a}$ in place of a. A similar argument can be made for right-hand tail probabilities. With $a = \sigma_{\eta_l}/\sigma_\varphi$, a lower bound for a is obtained when σ_{η_l} is replaced by $\underline{\sigma}_{\eta_l}$ and σ_φ is replaced by $\bar{\sigma}_\varphi$, as stated. Therefore, a S.O for φ when σ_{η_l} and σ_φ are unknown is given by

$$\bar{p}_\varphi(\varphi) = \frac{\underline{\sigma}_{\eta_l}}{\bar{\sigma}_\varphi} \bar{p}_{\eta_l}\left(\frac{\underline{\sigma}_{\eta_l}}{\bar{\sigma}_\varphi}\varphi\right) \tag{10}$$

To summarize, $\bar{p}_{\eta_l}(\eta_l)$, $\underline{\sigma}_{\eta_l}$ and $\bar{\sigma}_\varphi$ must be determined for each $\boldsymbol{\eta}_{ik}$ and used in Eq. (10) to obtain $\bar{p}_\varphi(\varphi)$. The S.O's are then convolved to construct a CDF overbound on the desired state y_k.

Review of Assumptions

At this point, we have a semi-quantitative view of how to overbound KF-based estimate error distributions, but still need to discuss how the variance bounds $\underline{\sigma}_{\eta_l}$ and $\bar{\sigma}_\varphi$ are obtained. This will be covered in the next section. However, before we get there, it is instructive to review the underlying assumptions summarized below.

1) Independence among the components of $\boldsymbol{w}_k$ and $\boldsymbol{v}_k$.
2) Initial vector $\boldsymbol{e}_{0|0}$ is independent of all process and measurement noise components at any time.
3) The $\boldsymbol{\eta}_{ik}$ in Eq. (7) have zero-mean, symmetric, and unimodal probability distributions.
4) The $\boldsymbol{\eta}_{ik}$ can each be expressed as a linear transformation of a spherically symmetric random vector.
5) All process and measurement noise components are WSS random processes (will be important in the next section).

These assumptions must be validated or shown that they can be relaxed prior to using Eq. (10) as a basis for overbounding. We discussed earlier how the independence assumption in 2) can be relaxed. It may also be possible to relax the assumptions in 3) by using paired overbounding [9] to establish a convolutional connection between the overbounds $\bar{p}_\varphi(\varphi)$ and a CDF overbound on y_k. This is a topic for future work. With regards to the spherical symmetry assumption in 4), the transformation rule of probability says that the joint PDF of a random vector $\boldsymbol{x} = \mathbf{G}\boldsymbol{\zeta}$ is a function of $\boldsymbol{x}^T(\mathbf{G}\mathbf{G}^T)^{-1}\boldsymbol{x}$ (see Eq. 6-118 in [10]). That is, $\boldsymbol{x}$ has an elliptical distribution. Thus, one way to validate 4) is to test whether the $\boldsymbol{\eta}_{ik}$ have elliptic distributions. This is an area of active research and the reader is referred to [11] and the references within for information on testing for ellipticity. Tests for stationarity of time series have been well established, and an example of their use in GPS measurement error modeling can be found in [12].

VARIANCE BOUNDING

This section discusses how to determine the variance bounds $\underline{\sigma}_{\eta_l}$ and $\bar{\sigma}_\varphi$ in Eq. (10), which must be defined for each of the $\boldsymbol{\eta}_{ik}$ in Eq. (7). Appendix A shows that if a CDF *underbound* can be obtained for the distribution of a random variable x, then the variance of the underbound is a lower bound on the true variance. Reference [13] describes a method for deriving CDF overbounds from empirical datasets that can be applied "in reverse" to establish a CDF underbound. It is also important to point out that the underbounds can be determined offline. This cannot be said, however, for $\bar{\sigma}_\varphi$. Changes in the operating environment significantly impact the KF estimate error variance, and these changes cannot be abstracted away.

Consider, for example, satellite-based navigation applications where changes in satellite geometry are known to affect the positioning estimate error distribution. One might think that this effect can be captured using a geometry indicator like dilution of precision (DOP). However, this would be difficult for KFs because the filter maintains a memory, meaning that the estimate error distribution at any given time depends on the entire history of measurements. In other words, the estimate error distribution would have to be quantified over all possible DOP histories, which is intractable. Therefore, the bound $\bar{\sigma}_\varphi$ must be constructed in real-time during KF operation.

A significant practical difficulty with establishing $\bar{\sigma}_\varphi$ is that the bound must account for uncertainty in modeling measurement and process noise time-correlation. Until recently, the only approach available was to use Eq. (6) to derive an expression for the estimate error variance in terms of the input noise ACSs, and then use upper and lower bounds on the ACSs to obtain a variance bound $\bar{\sigma}_\varphi^2$ [6]. This approach has serious practical difficulties because, as we pointed out earlier, the matrices in Eq. (6) grow with each KF update. Thus, the scope of applications where the variance bound can be computed in real-time is

considerably narrow. Our recent publication [1] presents a new frequency-domain overbounding (F.D.O) method for obtaining $\bar{\sigma}_{\varphi}$ that addresses the practical difficulties in [6]. The main result in [1] is summarized below.

> *Suppose that the input noise components are wide sense stationary random processes. For a given component, let $\mathcal{F}(\Omega)$ be the Fourier transform of its autocorrelation sequence, windowed to lags within the KF duration. When noise models are specified so that their power spectral density (PSD) $P(\Omega) \geq \mathcal{F}(\Omega)$ for all Ω, the resulting KF covariance matrix is guaranteed to predict an estimate error variance greater than or equal to the true variance for any state of interest.*

F.D.O is a powerful result because it allows us to use simple models like the first-order Gauss-Markov (FOGM) model to account for correlated noise, even though the underlying process may not be FOGM. Furthermore, F.D.O leads to a recursive approach for obtaining the bound $\bar{\sigma}_{\varphi}$, eliminating the unbounded growth problem in [1]. Like the CDF underbounds, noise models that satisfy the criteria of F.D.O can be obtained offline. The implications of F.D.O are just beginning to be explored. For example, [14] uses F.D.O to derive tight bounds on uncertain FOGM noise. However, F.D.O is still largely a theoretical result. Procedures for defining noise models from experimental data remain to be specified and are actively being pursued (see [12] and [15]).

We summarize the offline modeling steps needed to implement S.O + F.D.O in Figure 1.

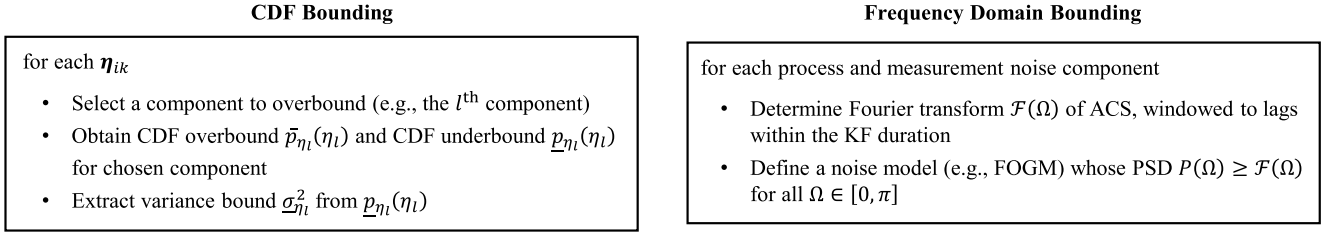

Figure 1. Offline modeling steps for symmetric and frequency domain overbounding.

Once models for correlated noise have been defined through F.D.O, they are incorporated in the KF through state augmentation. The models could also be incorporated using other means like measurement differencing described in [16]. However, we choose to focus on state augmentation given its common use in practice.

We have not discussed yet how to propagate the contribution of $\boldsymbol{e}_{0|0}$ and each process and measurement noise component to the KF covariance matrix $\boldsymbol{\Sigma}$. We propose using Eq. (5) for this task because it shows directly how each noise component maps into the error vector $\boldsymbol{e}$. Appendix B shows that the covariance matrix of $\boldsymbol{e}_{k|k}$, denoted as $\mathbf{P}_{k|k}$, can be written as

$$\mathbf{P}_{k|k} = (\boldsymbol{\Lambda}_{k|k})_{\text{init}} + \sum_{i=1}^{p} [\mathbf{I} \quad \mathbf{0}](\boldsymbol{\Lambda}_{k|k})_{w_i} \begin{bmatrix} \mathbf{I} \\ \mathbf{0} \end{bmatrix} + \sum_{j=1}^{s} [\mathbf{I} \quad \mathbf{0}](\boldsymbol{\Lambda}_{k|k})_{v_j} \begin{bmatrix} \mathbf{I} \\ \mathbf{0} \end{bmatrix} \tag{11}$$

The appendix also shows how to propagate the $\boldsymbol{\Lambda}$ matrices. For a given state $y_k = \boldsymbol{\alpha}_k^T \boldsymbol{x}_{k|k}$, the total estimate error variance bound is

$$\bar{\sigma}^2_{y_k} = \boldsymbol{\alpha}_k^T (\boldsymbol{\Lambda}_{k|k})_{\text{init}} \boldsymbol{\alpha}_k + \sum_{i=1}^{p} [\boldsymbol{\alpha}_k^T \quad \mathbf{0}](\boldsymbol{\Lambda}_{k|k})_{w_i} \begin{bmatrix} \boldsymbol{\alpha}_k \\ \mathbf{0} \end{bmatrix} + \sum_{j=1}^{s} [\boldsymbol{\alpha}_k^T \quad \mathbf{0}](\boldsymbol{\Lambda}_{k|k})_{v_j} \begin{bmatrix} \boldsymbol{\alpha}_k \\ \mathbf{0} \end{bmatrix} \tag{12}$$

The terms on the right-hand side of Eq. (12) are the contributions to $\bar{\sigma}^2_{y_k}$ from $\boldsymbol{e}_{0|0}$, and each process and measurement noise component that are used to determine the overbounds in Eq. (10).

In addition to propagating the KF covariance matrix $\boldsymbol{\Sigma}$, we must also propagate the $\boldsymbol{\Lambda}$'s to determine the variance bounds. However, as Appendix B shows, propagation of the $\boldsymbol{\Lambda}$'s is entirely recursive and only involves matrix multiplication. By combining F.D.O with S.O, we have, for the first time, a real-time feasible method to overbound KF-based estimate error distributions in the presence of time-correlated, non-Gaussian noise without requiring intimate knowledge of the underlying time correlation.

ILLUSTRATIVE EXAMPLE

In this section, we will demonstrate the overbounding method for a KF applied to the linear system

$$\begin{bmatrix} x_{k+1} \\ n_{k+1} \end{bmatrix} = \begin{bmatrix} 1 & 0 \\ 0 & 1 \end{bmatrix} \begin{bmatrix} x_k \\ n_k \end{bmatrix}$$
$$\begin{bmatrix} \rho_k \\ \phi_k \end{bmatrix} = \begin{bmatrix} 1 & 0 \\ 1 & 1 \end{bmatrix} \begin{bmatrix} x_k \\ n_k \end{bmatrix} + \begin{bmatrix} v_{\rho,k} \\ v_{\phi,k} \end{bmatrix} \quad (13)$$

Equation (13) is a simplified version of a static position estimation problem using GPS pseudorange and carrier phase measurements. In this analogy, ρ_k is the pseudorange measurement providing an unambiguous measurement of position x_k, and ϕ_k is the carrier phase measurement, which provides an ambiguous measurement of x_k due to the cycle ambiguity n_k. The discrete-time sampling interval Δt for the system in Eq. (13) is 1 second. Pseudorange and carrier phase measurement noise $v_{\rho,k}$ and $v_{\phi,k}$ are mutually independent but individually time correlated with the ACSs shown in Figure 2.

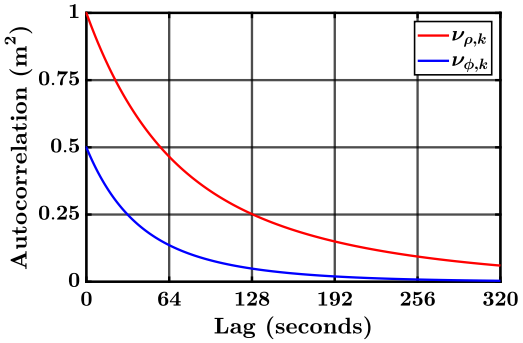

Measurement Noise	Autocorrelation Sequence
$v_{\rho,k}$	$0.5e^{-l\Delta t/150} + 0.5e^{-l\Delta t/50}$
$v_{\phi,k}$	$0.25e^{-l\Delta t/75} + 0.25e^{-l\Delta t/30}$

*$l\Delta t$ is the lag (in seconds) on the x-axis of the figure.

Figure 2. Pseudorange and carrier phase measurement noise ACSs.

Time Correlation Models

Figure 2 shows that each ACS is the sum of two FOGMs. For this example, the variances of $v_{\rho,k}$ and $v_{\phi,k}$ are known, but we do not exploit the mathematical structure in Figure 2. Instead, we will use F.D.O in this section to define FOGM models for pseudorange and carrier phase measurement error time correlation. The steps involved are summarized in Figure 3 for pseudorange measurement error.

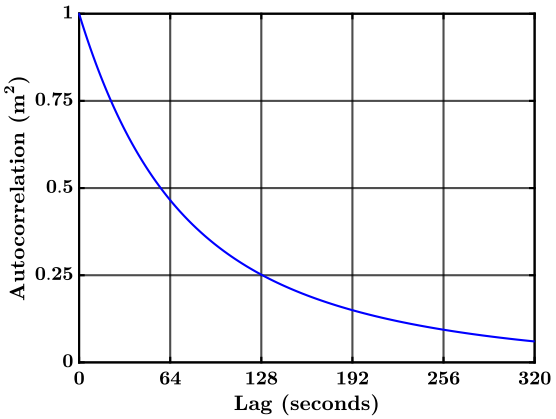

(a) Pseudorange ACS.

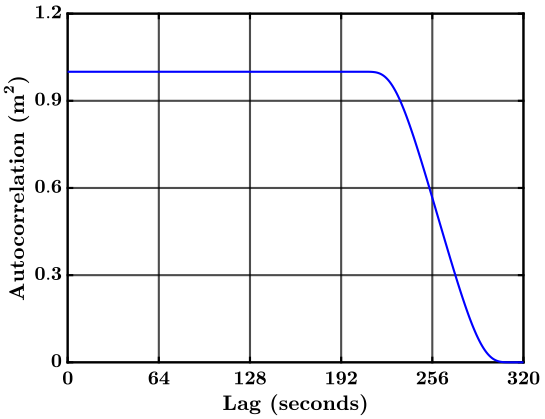

(b) Tapered window.

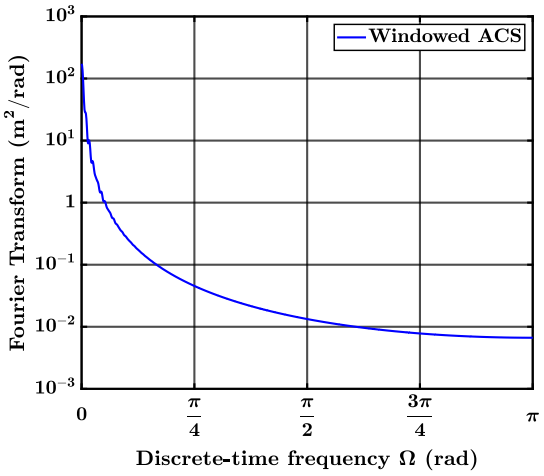

(c) Fourier transform of windowed pseudorange ACS.

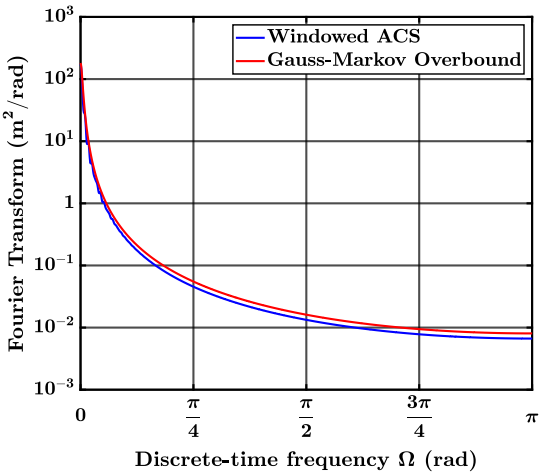

(d) Overbounding FOGM for pseudorange noise.

Figure 3. Pseudorange and carrier phase measurement noise ACSs.

Figure 3a shows again the raw pseudorange measurement noise ACS that was presented in Figure 2. For this example, the maximum KF duration is 200 seconds. Therefore, we attenuate the ACS to zero smoothly for lags beyond 200 seconds. This is achieved using the tapering window in Figure 3b, which is obtained using Eq. (12) in [1] with parameters $n = 200$ and $n_s = 320$. The reader should not confuse this value of n with the cycle ambiguity state n_k. After applying the tapered window to the ACS, we transform to the frequency domain using the Fourier transform. The result of this process is shown in Figure 3c. Lastly, we define a variance and time constant for a FOGM process so that its PSD is greater than or equal to the transformed ACS's value at all discrete-time frequencies Ω. The FOGM models obtained from this process are provided in Table 1 and are incorporated in the KF using state augmentation.

Table 1. First-order Gauss-Markov models obtained using F.D.O.

Measurement Noise	Variance ($\mathbf{m^2}$)	Time Constant (seconds)
Pseudorange	1.21	75
Carrier phase	0.58	45

Notice that the variances in Table 1 are inflated relative to the true variances in Figure 2 (1.0 m^2 for $\nu_{\rho,k}$ and 0.5 m^2 for $\nu_{\phi,k}$), despite the assumption that the measurement noise variances are known. This makes intuitive sense because a FOGM process is being used to model correlated noise that is not FOGM. While it may be easy to reach the conclusion that the variance of an inexact model should be inflated to account for model uncertainty, it is not easy to ascertain how much inflation is required. This is the power of F.D.O. It gives us a rigorous approach for determining the necessary amount of model inflation needed to account for the fact that the model does not match reality.

CDF Overbounds

The previous section described the frequency domain bounding column in Figure 1, and this section covers the CDF bounding column. According to Figure 1, we need to specify CDF overbounds for any component of $\boldsymbol{e}_{0|0}$, $\boldsymbol{\nu}_{\rho,K}$ and $\boldsymbol{\nu}_{\phi,K}$ (there is no process noise for this example). First, let us define the true distributions of these random vectors. Recall from the discussion after Eq. (4) that $\boldsymbol{e}_{0|0}^T = \left[\boldsymbol{\varepsilon}_{\xi,0}^T \quad \widehat{\boldsymbol{a}}_0^T\right]$, which, for this example, is the 4×1 Gaussian random vector $\boldsymbol{e}_{0|0}^T = [\varepsilon_{x,0} \quad \varepsilon_{n,0} \quad 0 \quad 0]$ with zero mean and known covariance matrix $\mathbf{P}_{0|0} = \text{diag}(10\ \text{m}^2, 10\ \text{m}^2, 0, 0)$. The two zeros in $\boldsymbol{e}_{0|0}$ are the initial estimates of the FOGM states included in the KF to account for time correlation. For the pseudorange and carrier phase measurement noise, we consider two cases. One where $\boldsymbol{\nu}_{\rho,K}$ and $\boldsymbol{\nu}_{\phi,K}$ are Gaussian distributed, and one where $\boldsymbol{\nu}_{\rho,K}$ is non-Gaussian and $\boldsymbol{\nu}_{\phi,K}$ is Gaussian. The PDFs of $\boldsymbol{e}_{0|0}$, $\boldsymbol{\nu}_{\rho,K}$ and $\boldsymbol{\nu}_{\phi,K}$ are summarized in Table 2 for both cases.

Table 2. Joint distributions of $\boldsymbol{e}_{0|0}$, $\boldsymbol{\nu}_{\rho,K}$ and $\boldsymbol{\nu}_{\phi,K}$.

Random Vector	Joint Probability Density Function	
	Case 1 (Gaussian)	Case 2 (Non-Gaussian)
$\boldsymbol{e}_{0\|0}$	$N(\mathbf{0}, \mathbf{P}_{0\|0})$	$N(\mathbf{0}, \mathbf{P}_{0\|0})$
$\boldsymbol{\nu}_{\rho,K}$	$N(\mathbf{0}, \mathbf{R}_{\rho})$	Linear transformation of multivariate T-distribution
$\boldsymbol{\nu}_{\phi,K}$	$N(\mathbf{0}, \mathbf{R}_{\phi})$	$N(\mathbf{0}, \mathbf{R}_{\phi})$

The matrices $\mathbf{R}_{\rho}$ and $\mathbf{R}_{\phi}$ are symmetric Toeplitz matrices with first columns (which completely define the matrices) populated using the formulas in Figure 2 with $l = 0, 1, 2, \ldots, 200$. For $\boldsymbol{\nu}_{\rho,K}$ in case 2, we define the vector as

$$\boldsymbol{\nu}_{\rho,K} = \mathbf{R}_{\rho}^{1/2} \left(\frac{m-2}{2}\right) \boldsymbol{t}_m(\mathbf{0}, \mathbf{I}) \tag{14}$$

such that $\boldsymbol{t}_m(\mathbf{0}, \mathbf{I})$ is a multivariate T-distribution with m degrees of freedom, zero-mean and covariance matrix $\left(\frac{m}{m-2}\right)\mathbf{I}$ [17]. The transformation $\mathbf{R}_{\rho}^{1/2}\left(\frac{m-2}{m}\right)$ ensures that the ACS of $\boldsymbol{\nu}_{\rho,K}$ has the structure in Figure 2. For this example, $m = 12$.

To define the CDF overbounds, we select the second component of $\boldsymbol{e}_{0|0}$ and the first components of both $\boldsymbol{\nu}_{\rho,K}$ and $\boldsymbol{\nu}_{\phi,K}$. We will use Gaussian overbounds due to their simplicity. For case 1 in Table 2, where all error sources are Gaussian, the CDF overbounds are identical to the true distributions because we assumed that the variances are known. For the non-Gaussian case, we simulated 4×10^7 instances of $\boldsymbol{\nu}_{\rho,K}$ in Eq. (14), computed the empirical CDF of the first component, and then determined the variance of a Gaussian overbound through trial and error. The empirical CDF and overbound are shown together in Figure 4 for the non-Gaussian pseudorange measurement error. Table 3 summarizes the CDF overbounds for the Gaussian and non-Gaussian cases.

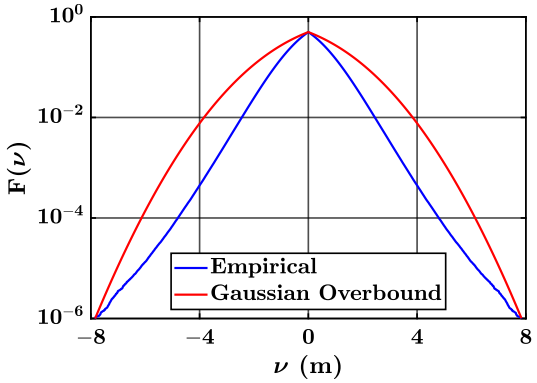

Figure 4. Pseudorange error folded CDF with Gaussian overbound for case 2 in Table 2.

Table 3. Gaussian overbounds.

Chosen Component to Overbound	Gaussian CDF Overbounds	
	Case 1 (Gaussian)	Case 2 (Non-Gaussian)
$\boldsymbol{e}_{0\|0}$	$N(0, 10\ \mathrm{m}^2)$	$N(0, 10\ \mathrm{m}^2)$
First component of $\boldsymbol{\nu}_{\rho,K}$	$N(0, 1.0\ \mathrm{m}^2)$	$N(0, 2.72\ \mathrm{m}^2)$
First component of $\boldsymbol{\nu}_{\phi,K}$	$N(0, 0.5\ \mathrm{m}^2)$	$N(0, 0.5\ \mathrm{m}^2)$

Overbounding Results

Overbounding results are presented in this section for the two cases shown in Table 2. Since we will be dealing with non-Gaussian noise, the demonstration will be accomplished using Monte Carlo simulation. Twenty million trials are run where measurement time series are generated with the appropriate noise statistics and processed by the KF. Position estimate error samples are collected at an elapsed time of 150 seconds, from which we form an empirical folded CDF that can be compared with the overbound obtained from our new method. To generate the non-Gaussian pseudorange measurement noise, we use Eq. (14) with $\boldsymbol{t}_m(\mathbf{0}, \mathbf{I})$ constructed using the method in [18].

Figure 5 shows the results for case 1 where all distributions are Gaussian. The empirical folded CDF is in red, the CDF overbound based solely on the F.D.O-derived variance bound is in blue, and the CDF overbound using our new method that combines S.O and F.D.O is shown in green. For this case, S.O offers no benefit over what was already achieved using F.D.O. This should not come as a surprise because in the Gaussian case, the variance bound provided by F.D.O is sufficient to overbound the estimate error distribution.

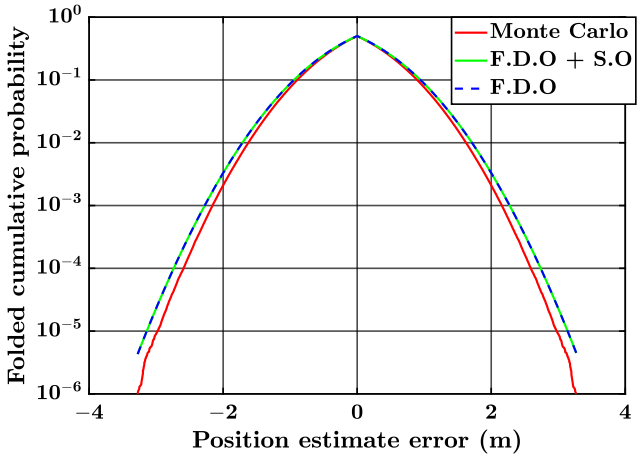

Figure 5. Position estimate error folded CDF with overbounds at elapsed time of 150 seconds: Gaussian case.

An entirely different outcome is observed in Figure 6 when the pseudorange measurement noise is non-Gaussian. In this scenario, F.D.O in isolation is not sufficient to overbound the position estimate error distribution, which can be seen in the tails of the folded CDF. As before, this should not be surprising since a variance bound is not sufficient to overbound the entire distribution for the general case of non-Gaussian noise. S.O provides the necessary inflation of the F.D.O-derived folded CDF above the empirical CDF, thereby resulting in an overbound on the entire estimate error distribution.

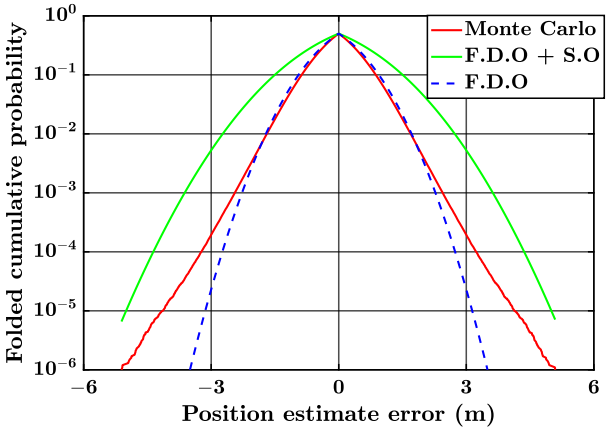

Figure 6. Position estimate error folded CDF with overbounds at elapsed time of 150 seconds: non-Gaussian case.

CONCLUSIONS

This paper presented a new method to overbound sequential estimation errors in the presence of time-correlated, non-Gaussian noise. The method combined symmetric overbounding and frequency domain overbounding, two approaches developed separately in the literature. We showed that F.D.O provides the key to making S.O practical and feasible as a real-time bounding algorithm. The new method was demonstrated for a simple GPS-based estimation problem where we showed the benefit of S.O in a non-Gaussian noise case. Work is ongoing on the practical aspects of obtaining frequency domain overbounds from experimental data and should continue to be a top priority of future work. Another topic for future study includes developing general approaches to test the feasibility of assumptions used in developing the method (i.e., ellipticity and wide sense stationarity). We also do not have a clear picture of the level of conservatism in the proposed method. Thus, it is crucial to investigate the implications of S.O + F.D.O in the context of an existing program like ARAIM.

APPENDIX A: VARIANCE OF CDF UNDERBOUND

This Appendix shows that for a zero-mean, symmetric and unimodal distribution, the variance of a CDF underbound is a lower bound on the true variance, provided that the overbound is also zero-mean, symmetric and unimodal. The fundamental definition of variance is

$$\sigma^2 = \int_{-\infty}^{\infty} x^2 f(x) dx = 2 \int_{-\infty}^{0} x^2 f(x) dx \tag{A1}$$

where we have used the fact that $f(x)$ is a zero-mean and symmetric distribution. Integrating by parts yields

$$\begin{aligned} \sigma^2 &= 2x^2 F(x)|_{-\infty}^{0} - 4 \int_{-\infty}^{0} xF(x) dx \\ &= -2\left[\lim_{x \to -\infty} x^2 F(x)\right] - 4 \int_{-\infty}^{0} xF(x) dx \end{aligned} \tag{A2}$$

Note that for any cumulative distribution function, $\lim_{x \to -\infty} F(x) = 0$. There are three cases to consider with regards to the limit in Eq. (A2). One where $F(x)$ decays at a rate slower than x^{-2}, a second where $F(x)$ decays like x^{-2} and a third where $F(x)$ decays quicker than x^{-2}. In the first case, the limit is ∞ because x^2 grows quicker than the rate at which $F(x)$ decays, resulting in an infinite variance. This is a degenerate case that will not be considered. In the second case, the limit is finite, but the integral has the form $\int_{-\infty}^{0} dx/x$, which we know diverges. Thus, the second case also produces an infinite variance and is degenerate. The only interesting scenario is the third one, where the limit evaluates to zero and the integrand has a decay rate of at least x^{-2}, resulting in a convergent integral. Therefore, Eq. (A2) simplifies to

$$\sigma^2 = -4 \int_{-\infty}^{0} xF(x) dx \tag{A3}$$

Suppose now that we replace $F(x)$ with a CDF underbound $\underline{F}(x)$, resulting in the new variance $\underline{\sigma}^2 = -4 \int_{-\infty}^{0} x\underline{F}(x) dx$. It can be shown that $(\underline{\sigma}^2 - \sigma^2) \leq 0$ (i.e., $\underline{\sigma}^2$ is less than or equal to σ^2) by using the fact that a CDF underbound is one where $\underline{F}(x) \leq F(x)$ when $x \leq 0$. That is,

$$\underline{\sigma}^2 - \sigma^2 = -4 \int_{-\infty}^{0} x\left[\underline{F}(x) - F(x)\right] dx \leq 0 \tag{A4}$$

where the inequality follows from the fact that the integrand is strictly nonnegative on the interval $(-\infty, 0]$. Thus, a lower bound on the variance of a random variable x can be obtained by defining a CDF underbound on the distribution of x.

APPENDIX B: PROPAGATING INDIVIDUAL CONTRIBUTIONS TO ESTIMATE ERROR COVARIANCE

This Appendix develops a propagation algorithm by walking through initialization and the first time and measurement updates of Eq. (5). To begin, let's write the initial vector $\boldsymbol{e}_{0|0}$ as a sum of contributions

$$\boldsymbol{e}_{0|0} = (\boldsymbol{e}_{0|0})_{\text{init}} + \sum_{i=1}^{p} [\mathbf{I} \quad \mathbf{0}] \begin{bmatrix} (\boldsymbol{e}_{0|0})_{w_i} \\ \boldsymbol{a}_{w_i,0} \end{bmatrix} + \sum_{j=1}^{s} [\mathbf{I} \quad \mathbf{0}] \begin{bmatrix} (\boldsymbol{e}_{0|0})_{v_j} \\ \boldsymbol{a}_{v_j,0} \end{bmatrix} \tag{B1}$$

where $(\boldsymbol{e}_{0|0})_{\text{init}}$ is the contribution from initialization steps that are independent of process and measurement noise, $(\boldsymbol{e}_{0|0})_{w_i}$ is the contribution from the i^{th} process noise component w_i, and $\boldsymbol{a}_{w_i,0}$ is a vector of augmented states for w_i at time index 0. Similar definitions exist for $(\boldsymbol{e}_{0|0})_{v_j}$ and $\boldsymbol{a}_{v_j,0}$.

Recall that we are focused on the specific case where $\boldsymbol{e}$ is initialized independent of process and measurement noise. Therefore, $(\boldsymbol{e}_{0|0})_{w_i}$ and $(\boldsymbol{e}_{0|0})_{v_j}$ are zero vectors, and the covariance matrices $(\boldsymbol{\Lambda}_{0|0})_{w_i}$ and $(\boldsymbol{\Lambda}_{0|0})_{v_j}$ associated with $[(\boldsymbol{e}_{0|0}^T)_{w_i} \quad \boldsymbol{a}_{w_i,0}^T]$ and $[(\boldsymbol{e}_{0|0}^T)_{v_j} \quad \boldsymbol{a}_{v_j,0}^T]$ are

$$(\boldsymbol{\Lambda}_{0|0})_{w_i} = \begin{bmatrix} \mathbf{0} & \mathbf{0} \\ \mathbf{0} & E[\boldsymbol{a}_{w_i,0}\boldsymbol{a}_{w_i,0}^T] \end{bmatrix} \quad \text{and} \quad (\boldsymbol{\Lambda}_{0|0})_{v_j} = \begin{bmatrix} \mathbf{0} & \mathbf{0} \\ \mathbf{0} & E[\boldsymbol{a}_{v_j,0}\boldsymbol{a}_{v_j,0}^T] \end{bmatrix} \tag{B2}$$

Furthermore, since $\boldsymbol{e}_{0|0}$ is entirely defined by $(\boldsymbol{e}_{0|0})_{\text{init}}$, the covariance matrix $(\boldsymbol{\Lambda}_{0|0})_{\text{init}}$ associated with $(\boldsymbol{e}_{0|0})_{\text{init}}$ is equal to the initial covariance matrix $\mathbf{P}_{0|0}$. Next, we will show how to update the $\boldsymbol{\Lambda}$ matrices after the time update in Eq. (5), which is written below in a slightly different form

$$\boldsymbol{e}_{1|0} = \mathbf{F}_0 \boldsymbol{e}_{0|0} - \begin{bmatrix} \boldsymbol{b}_{1,0} \\ \mathbf{0} \end{bmatrix} w_{1,0} - \cdots - \begin{bmatrix} \boldsymbol{b}_{p,0} \\ \mathbf{0} \end{bmatrix} w_{p,0} \tag{B3}$$

such that $\boldsymbol{b}_{i,0}$ is the i^{th} column of $\mathbf{B}_0$. In what follows, the subscripts i and j will be dropped to indicate that we are talking about arbitrary noise components. Update equations for $(\boldsymbol{e}_{0|0})_{\text{init}}$, $[(\boldsymbol{e}_{0|0}^T)_w \quad \boldsymbol{a}_{w,0}^T]$ and $[(\boldsymbol{e}_{0|0}^T)_v \quad \boldsymbol{a}_{v,0}^T]$ are obtained by substituting Eq. (B1) into Eq. (B3). For $(\boldsymbol{e}_{0|0})_{\text{init}}$, the update equation is simply

$$(\boldsymbol{e}_{1|0})_{\text{init}} = \mathbf{F}_0 (\boldsymbol{e}_{0|0})_{\text{init}} \tag{B4}$$

For an arbitrary process noise component, state augmentation allows us to write $w_0 = \boldsymbol{s}_{w,0}^T \boldsymbol{a}_{w,0} + n_0$, where $\boldsymbol{a}_w$ propagates according to $\boldsymbol{a}_{w,1} = \mathbf{L}_{w,0}\boldsymbol{a}_{w,0} + \boldsymbol{u}_{w,0}$. Thus, when a process noise component passes through Eq. (B3), we arrive at the update equation

$$\begin{bmatrix} (\boldsymbol{e}_{1|0})_w \\ \boldsymbol{a}_{w,1} \end{bmatrix} = \begin{bmatrix} \mathbf{F}_0 & -\boldsymbol{b}_0 \boldsymbol{s}_{w,0}^T \\ \mathbf{0} & \mathbf{L}_{w,0} \end{bmatrix} \begin{bmatrix} (\boldsymbol{e}_{0|0})_w \\ \boldsymbol{a}_{w,0} \end{bmatrix} + \begin{bmatrix} -\boldsymbol{b}_0 & \mathbf{0} \\ \mathbf{0} & \mathbf{I} \end{bmatrix} \begin{bmatrix} n_0 \\ \boldsymbol{u}_{w,0} \end{bmatrix} \tag{B5}$$

Similarly, for an arbitrary measurement noise component, we can write the update equation as

$$\begin{bmatrix} (\boldsymbol{e}_{1|0})_v \\ \boldsymbol{a}_{v,1} \end{bmatrix} = \begin{bmatrix} \mathbf{F}_0 & \mathbf{0} \\ \mathbf{0} & \mathbf{L}_{v,0} \end{bmatrix} \begin{bmatrix} (\boldsymbol{e}_{0|0})_v \\ \boldsymbol{a}_{v,0} \end{bmatrix} + \begin{bmatrix} \mathbf{0} \\ \mathbf{I} \end{bmatrix} \boldsymbol{u}_{v,0} \tag{B6}$$

After applying Eqs. (B5) and (B6) to each process and measurement noise component, Eq. (B3) can be written in the same form as Eq. (B1), i.e.,

$$\boldsymbol{e}_{1|0} = (\boldsymbol{e}_{1|0})_{\text{init}} + \sum_{i=1}^{p} [\mathbf{I} \quad \mathbf{0}] \begin{bmatrix} (\boldsymbol{e}_{1|0})_{w_i} \\ \boldsymbol{a}_{w_i,1} \end{bmatrix} + \sum_{j=1}^{s} [\mathbf{I} \quad \mathbf{0}] \begin{bmatrix} (\boldsymbol{e}_{1|0})_{v_j} \\ \boldsymbol{a}_{v_j,1} \end{bmatrix} \tag{B7}$$

Taking expected values of Eqs. (B4)-(B6) results in the covariance updates

$$
\begin{aligned}
(\boldsymbol{\Lambda}_{1|0})_{\text{init}} &= \mathbf{F}_0(\boldsymbol{\Lambda}_{0|0})_{\text{init}}\mathbf{F}_0^T \\
(\boldsymbol{\Lambda}_{1|0})_w &= \begin{bmatrix}\mathbf{F}_0 & -\boldsymbol{b}_0\boldsymbol{s}_{w,0}^T \\ \mathbf{0} & \mathbf{L}_{w,0}\end{bmatrix}(\boldsymbol{\Lambda}_{0|0})_w\begin{bmatrix}\mathbf{F}_0 & -\boldsymbol{b}_0\boldsymbol{s}_{w,0}^T \\ \mathbf{0} & \mathbf{L}_{w,0}\end{bmatrix}^T + \begin{bmatrix}\boldsymbol{b}_0\boldsymbol{b}_0^T\sigma_{n,0}^2 & \mathbf{0} \\ \mathbf{0} & \mathbf{U}_{w,0}\end{bmatrix} \\
(\boldsymbol{\Lambda}_{1|0})_v &= \begin{bmatrix}\mathbf{F}_0 & \mathbf{0} \\ \mathbf{0} & \mathbf{L}_{v,0}\end{bmatrix}(\boldsymbol{\Lambda}_{0|0})_v\begin{bmatrix}\mathbf{F}_0^T & \mathbf{0} \\ \mathbf{0} & \mathbf{L}_{v,0}^T\end{bmatrix} + \begin{bmatrix}\mathbf{0} & \mathbf{0} \\ \mathbf{0} & \mathbf{U}_{v,0}\end{bmatrix}
\end{aligned}
\tag{B8}
$$

A similar process can be followed when going through the measurement update in Eq. (5), written below in a slightly different form

$$
\boldsymbol{e}_{1|1} = (\mathbf{I} - \mathbf{K}_1\mathbf{H}_1)\boldsymbol{e}_{1|0} + \mathbf{K}_1\boldsymbol{d}_{1,1}\nu_1 + \cdots + \mathbf{K}_1\boldsymbol{d}_{s,1}\nu_s \tag{B9}
$$

where $\boldsymbol{d}_{j,1}$ is the j^{th} column of $\mathbf{D}_1$. Substituting Eq. (B7) into Eq. (B9) leads to the following update equations for $(\boldsymbol{e}_{1|0})_{\text{init}}$ and an arbitrary component of process and measurement noise

$$
(\boldsymbol{e}_{1|1})_{\text{init}} = (\mathbf{I} - \mathbf{K}_1\mathbf{H}_1)(\boldsymbol{e}_{1|0})_{\text{init}} \tag{B10a}
$$

$$
\begin{bmatrix}(\boldsymbol{e}_{1|1})_w \\ \boldsymbol{a}_{w,1}\end{bmatrix} = \begin{bmatrix}\mathbf{I} - \mathbf{K}_1\mathbf{H}_1 & \mathbf{0} \\ \mathbf{0} & \mathbf{I}\end{bmatrix}\begin{bmatrix}(\boldsymbol{e}_{1|0})_w \\ \boldsymbol{a}_{w,1}\end{bmatrix} \tag{B10b}
$$

$$
\begin{bmatrix}(\boldsymbol{e}_{1|1})_v \\ \boldsymbol{a}_{v,1}\end{bmatrix} = \begin{bmatrix}\mathbf{I} - \mathbf{K}_1\mathbf{H}_1 & \mathbf{K}_1\boldsymbol{d}_1\boldsymbol{s}_{v,1}^T \\ \mathbf{0} & \mathbf{I}\end{bmatrix}\begin{bmatrix}(\boldsymbol{e}_{1|0})_v \\ \boldsymbol{a}_{v,1}\end{bmatrix} + \begin{bmatrix}\mathbf{K}_1\boldsymbol{d}_1 \\ \mathbf{0}\end{bmatrix}r_1 \tag{B10c}
$$

where we have incorporated the augmentation model $\nu_1 = \boldsymbol{s}_{v,1}^T\boldsymbol{a}_{v,1} + r_1$ for an arbitrary measurement noise component. After applying Eqs. (B10b) and (B10c) to each process and measurement noise component, the measurement update in Eq. (B9) can be written as

$$
\boldsymbol{e}_{1|1} = (\boldsymbol{e}_{1|1})_{\text{init}} + \sum_{i=1}^{p}[\mathbf{I} \quad \mathbf{0}]\begin{bmatrix}(\boldsymbol{e}_{1|1})_{w_i} \\ \boldsymbol{a}_{w_i,1}\end{bmatrix} + \sum_{j=1}^{s}[\mathbf{I} \quad \mathbf{0}]\begin{bmatrix}(\boldsymbol{e}_{1|1})_{v_j} \\ \boldsymbol{a}_{v_j,1}\end{bmatrix} \tag{B11}
$$

Taking expected values of Eqs. (B10a)-(B10c) results in the covariance updates

$$
\begin{aligned}
(\boldsymbol{\Lambda}_{1|1})_{\text{init}} &= (\mathbf{I} - \mathbf{K}_1\mathbf{H}_1)(\boldsymbol{\Lambda}_{1|0})_{\text{init}}(\mathbf{I} - \mathbf{K}_1\mathbf{H}_1)^T \\
(\boldsymbol{\Lambda}_{1|1})_w &= \begin{bmatrix}\mathbf{I} - \mathbf{K}_1\mathbf{H}_1 & \mathbf{0} \\ \mathbf{0} & \mathbf{I}\end{bmatrix}(\boldsymbol{\Lambda}_{1|0})_w\begin{bmatrix}\mathbf{I} - \mathbf{K}_1\mathbf{H}_1 & \mathbf{0} \\ \mathbf{0} & \mathbf{I}\end{bmatrix}^T \\
(\boldsymbol{\Lambda}_{1|1})_v &= \begin{bmatrix}\mathbf{I} - \mathbf{K}_1\mathbf{H}_1 & \mathbf{K}_1\boldsymbol{d}_1\boldsymbol{s}_{v,1}^T \\ \mathbf{0} & \mathbf{I}\end{bmatrix}(\boldsymbol{\Lambda}_{1|0})_v\begin{bmatrix}\mathbf{I} - \mathbf{K}_1\mathbf{H}_1 & \mathbf{K}_1\boldsymbol{d}_1\boldsymbol{s}_{v,1}^T \\ \mathbf{0} & \mathbf{I}\end{bmatrix} + \begin{bmatrix}\mathbf{K}_1\boldsymbol{d}_1\boldsymbol{d}_1^T\mathbf{K}_1^T\sigma_{r,1}^2 & \mathbf{0} \\ \mathbf{0} & \mathbf{0}\end{bmatrix}
\end{aligned}
\tag{B12}
$$

The process continues during the next time update. Equations (B2), (B8) and (B12) are the propagation equations needed to determine individual contributions to the estimate error variance bound.

REFERENCES

1. Langel S., Garcia-Crespillo, O., and Joerger, M., "A New Approach for Modeling Correlated Gaussian Errors Using Frequency Domain Overbounding," *Proceedings of the 2020 IEEE/ION Position, Location and Navigation Symposium (PLANS 2020), Portland, OR, April 2020*, pp. 868-876.
2. Rife, J. and Gebre-Egziabher, D., "Symmetric Overbounding of Correlated Errors," *NAVIGATION*, Vol. 54, 2007, pp. 109-124.
3. Joerger, M. and Pervan, B., "Exploiting Satellite Motion in ARAIM: Measurement Error Model Refinement Using Experimental Data," *Proceedings of the 29th International Technical Meeting of the Satellite Division of the Institute of Navigation (ION GNSS+ 2016), Portland, OR, September 2016*, pp. 1696-1712.
4. Pervan, B., Khanafseh, S., and Patel, J., "Test Statistic Auto- and Cross-correlation Effects on Monitor False Alert and Missed Detection Probabilities," *Proceedings of the 2017 International Technical Meeting of the Institute of Navigation (ITM 2017), Monterey, CA, January 2017*, pp. 562-590.
5. Langel, S., Khanafseh, S., and Pervan, B., "Bounding Integrity Risk for Sequential State Estimators with Stochastic Modeling Uncertainty," *AIAA Journal of Guidance, Control, and Dynamics*, Vol, 37, 2014, pp. 36-46.
6. Langel, S., Khanafseh, S., and Pervan, B., "Bounding Integrity Risk Subject to Structured Time Correlation Modeling Uncertainty," Proceedings of the 2012 *IEEE/ION Position, Location and Navigation Symposium (PLANS 2012), Myrtle Beach, SC, April 2012*, pp. 678-684.
7. Anderson, B. D. O. and Moore, J. B., *Optimal Filtering*, Dover Publications, Inc., Mineola, NY, 1979, pp. 288-290.
8. DeCleene, B., "Defining Pseudorange Integity – Overbounding," *Proceedings of the 13th International Technical Meeting of the Satellite Division of the Institute of Navigation (ION GPS 2000), Salt Lake City, UT, September 2000*, pp. 1916-1924.
9. Rife, J., Pullen S., Enge, P., and Pervan, B., "Paired Overbounding for Nonideal LAAS and WAAS Error Distributions," *IEEE Transactions on Aerospace and Electronic Systems*, Vol. 42, 2006, pp. 1386-1395.
10. Papoulis, A. and Pillai, S. U., *Probability, Random Variables, and Stochastic Processes*, 4th ed., McGraw-Hill, New York, NY, 2002, pp. 201.
11. Babic, S., Gelbgras, L., Hallin, M., and Ley, C., "Optimal Tests for Elliptical Symmetry: Specified and Unspecified Location," *arXiv*:1911.08171v1 [stat.ME], 2019.
12. Gallon, E., Joerger, M., and Pervan, B., "Frequency-Domain Modeling of Orbit and Clock Errors for Sequential Positioning," *Proceedings of the 33rd International Technical Meeting of the Satellite Division of the Institute of Navigation (ION GNSS+ 2020), St. Louis, MO, September 2020*.
13. Blanch, J., Walter, T., and Enge, P., "A MATLAB Toolset to Determine Strict Gaussian Bounding Distributions of a Sample Distribution," *Proceedings of the 30th International Technical Meeting of the Satellite Division of the Institute of Navigation (ION GNSS+ 2017), Portland, OR, September 2017*, pp. 4236-4247.
14. Garcia Crespillo, O., Joerger, M., and Langel, S., "Tight Bounds for Uncertain Time-Correlated Errors with Gauss-Markov Structure," *arXiv*:2009.09495 [eess.SP], 2020.
15. Jada, S. K. and Joerger, M., "GMP-Overbound Parameter Determination for Measurement Error Time Correlation Modeling," *Proceedings of the 2020 International Technical Meeting of the Institute of Navigation, San Diego, CA, January 2020*, pp. 189-206.
16. Bryson, A. E., and Henrikson, L. J., "Estimation Using Sampled Data Containing Sequentially Correlated Noise," *Journal of Spacecraft and Rockets*, Vol. 5, 1968, pp. 662-665.
17. Lin, P. E., "Some Characterizations of the Multivariate t Distribution," *Journal of Multivariate Analysis*, Vol. 2, 1972, pp. 339-344.
18. Boisbunon, A., "The Class of Multivariate Spherically Symmetric Distributions," *Technical Report* #2012-005, 2012.